Journal of Robotics and Control (JRC)
Volume 5, Issue 2, 2024
ISSN: 2715-5072, DOI: 10.18196/jrc.v5i2.21127

Soft Actuator Based on a Novel Variable Stiffness Compound Extensor Bending-Pneumatic Artificial Muscle (CEB-PAM): Design and Mathematical Model

Wafaa Al-Mayahi [1]*, Hassanin Al-Fahaam [2]
[1, 2] Department of Computer Engineering, University of Basrah, Basrah, Iraq
Email: [1] engpg.wafaa.daraj@uobasrah.edu.iq, [2] hassanin.husein@uobasrah.edu.iq
*Corresponding Author

***Abstract*—Soft robots have gained prominence in various fields in recent years, particularly in medical applications such as rehabilitation, due to their numerous advantages. The primary building blocks of a soft robot are often pneumatic artificial muscles (PAM). The Extensor PAM (EPAM), including Extensor Bending PAM (EB-PAM), is characterized by its low stiffness, and because stiffness is important in many robotic applications, for example, in rehabilitation, the degree of disability varies from one person to another, such as spasticity, weakness, and contracture. Therefore, it was necessary to provide an actuator with variable stiffness whose stiffness can be controlled to provide the appropriate need for each person, this study presents a new design for the EB-PAM that combines the EB-PAM and contractor PAM (CPAM), It has higher stiffness than traditional EPAM, A stiffness of over 850 N/m was achieved, whereas EB-PAM only reached a stiffness of less than 450 N/m, it is also possible to change its stiffness at a specific bending angle. It is also possible to obtain fixed stiffness at different angles. A mathematical model was developed to calculate the output force of the new muscle by calculating its size and the pressure applied to it and comparing the model with experimental results. The mathematical model was enhanced by calculating the wasted energy consumed by the actuator before the bladder begins to expand, and also by calculating the thickness of the bladder and the sleeve. To make the muscle lighter, cheaper, and work under low pressures, balloons were used in manufacturing, offering practical advantages for soft robotic applications.**

Keywords—Soft Robot; Soft Actuator; Pneumatic Artificial Muscle (PAM); Variable Stiffness; Extensor Bending Muscle.

I. INTRODUCTION

Due to the numerous advantages of PAM, such as their high degree of freedom [1][2], compliance, low cost [3][4], and safety in direct interaction with humans [5]-[7], they have been used in the soft robots that assist in the rehabilitation of disabled individuals with neurological damage or the elderly with physical weakness [8]-[11]. However, rigid robots are not appropriate for such applications [12][13], as they require complex mechanical structures and feedback systems to prevent accidental damage [14]-[17]. Also, soft robots have an advantage over rigid robots; they produce small resistance to obstacles and can adapt easily [18][19], allowing them to handle soft and fragile loads without undergoing any damage [20][21]. Furthermore, an individual can be accommodated with soft robots without requiring extensive adjustment or calibration [22]-[24]. Additionally, they are simple to use and portable, Therefore, these robots have drawn researchers' interest in different fields, such as biology, physics, material science, and computer and control engineering [24]-[29].

PAM, also known as the McKibben muscle [30][31], Which is the basic building block of the soft robot [32], is made of soft materials such as rubber tubes that represent bladders and braided sleeves that are fixed with rigid caps at both ends to prevent air leakage [33]-[36]. When pressure is applied to these tubes, they can contract or expand, producing a pulling or pushing force [1][8][37]. The type of actuator is determined by the length of the tube and sleeve [38][39]. When the sleeve is longer than the bladder, meaning that the angle formed between the threads of the sleeve is smaller than 54.7°, the muscle will be CPAM, and when pressure is applied to it, it will contract to generate a pulling force [40]-[42]. However, if the angle generated between the threads of the sleeve is greater than 54.7°, then the muscle is categorized as an EPAM, and when pressure is applied to it, it will extend and generate a pushing force. From a CPAM or EPAM muscle, an extensor bending (EB-PAM) or Contractor bending (CB-PAM) can be generated [24][43][44].

For finger-like devices, such as grippers or prosthetic hands, EBPAM has been manufactured so that one side has more expansion than the other [45][46]. To form it, an elastic frame is inserted between the elastic tube and the braid to cause lateral deformation and fixed with the end fittings, which were designed to characterize the mechanical characteristics of the actuator [47]-[49]. The flexible frame can increase the stability and bearing capacity by preventing breakdown under side loads [14][50]-[53]. Similarly, by adjusting the braid angle, BPAM could be adjusted to either CB-PAM or EB-PAM. When comparing their performance, CB-PAM showed high output capacity and efficiency, while EB-PAM demonstrated large deformation over a wide range and outstanding compliance [21][54][55]. In addition, EB-PAM has a relatively low stiffness while CB-PAMs have higher stiffness and are less prone to deformation [34][43]. The low stiffness in the EB-PAM is due to misalignment [56] Furthermore, helical expanding PAM and helical contracting PAM were formed [57][58].

Some studies examined the impact of braid angle, radius, and internal volume on general bending motion. The CPAM, whether axial, helical, or bending, showed greater force and less deformation than the extensor one [59][60]. Al-Abadi [61] used a 3D-printed rod with a set of small holes along it is used to create CB-PAM. The rod is sewn onto the actuator outer cover and inserted between the rubber tube and the covered shell. It allows the actuator to freely contract from all sides while preventing contraction of the length. This causes the actuator to bend; however, the rod reduces the PMA softness, so the rigid rod was replaced with a flexible one [61]-[63].

Al-Fahaam [26] presented a mathematical model to calculate the force of EB-PAM. He made several enhancements to his model to reduce the difference between the mathematical model and the experimental results. He used the EB-PAM design which involves free one side and reinforcement of the other side with a thread to keep it from extending. Al-Mayahi [56] explained the extent to which the material used and the thickness of the bladder affects the rate of expansion and contraction, as he found that the muscle made of the balloon expands or contracts at the same rate compared to the muscle made of tube when half the amount of pressure is applied to the muscle. He additionally developed a muscle with high stiffness, capable of changing its stiffness at a particular length or maintaining stiffness at different lengths.

As EB-PAM was found to be less resistant to load increase, its ability to maintain the bending angle decreases; in other words, it has low stiffness [64][65], and because increasing and controlling stiffness is important in various robotic applications [66][67], for example, in the rehabilitation of limbs, variable stiffness helps more in rehabilitation, as the degree of stiffness or spasticity varies from one person to another, and the degree in the same disabled person can vary from one hand to another or from one finger to another in the same hand, which arose the need for an actuator with variable stiffness whose stiffness can be controlled according to the appropriate need for each person [68]-[70]. By using the Al-Fahham model of the EP-PAM [26] and mathematical analysis of the CPAM [56], the mathematical model of the new muscle was created, as previous models did not provide a bendable muscle whose stiffness could be controlled. Thus, this study introduces a new muscle design, made of balloon combining CPAM and EPAM, which is anticipated to offer enhanced load resistance and stiffness compared to conventional EB-PAM, it is also lighter in weight and less expensive.

The primary divisions of this paper can be encapsulated as follows: the design of the CPAM, the design of the EPAM, and the design particulars of the EB-PAM, and then, provides the design of the novel compound extensor bending-PAM (CEB-PAM) and how to achieve experimental results for stiffness through several experiments, followed by the mathematical model for calculating force through several mathematical coefficients linking force, volume, and pressure, making improvements to this model and comparing the mathematical results with experimental results to prove its validity. The research methodology flowchart is depicted in Fig. 1.

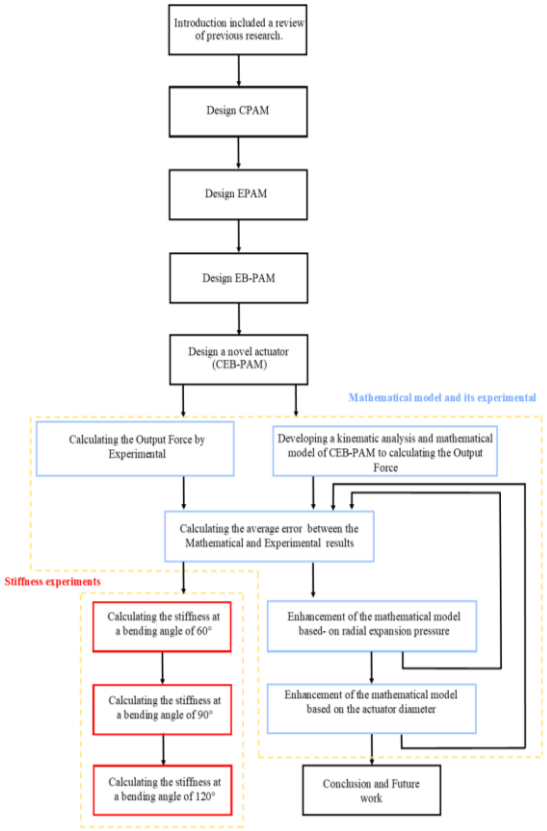

Fig. 1. A flow chart depicting the steps of the research methodology

II. CONTRACTION PNEUMATIC ARTIFICIAL MUSCLE

The contractile muscle (CPAM) was made up of a balloon bladder, a braided nylon sleeve that has the same length and diameter as the bladder (the length is 19.5 cm and the diameter is 0.5 cm), and two 3D-printed ends: one has a port allowing air to input and output from the muscle, while the other is closed as illustrated in Fig. 2. The muscle began to contract when air pressure is applied, and as the pressure increased, the diameter also increased causing the angle between the thread of the sleeve and the vertical axis to increase until it reached 54.7°. The muscle reaches its maximum contraction at this angle as illustrated in Fig. 3.

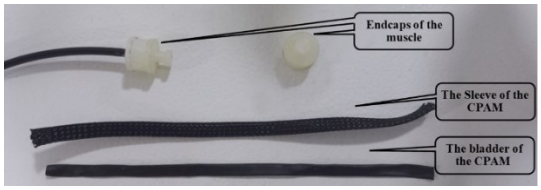

Fig. 2. The main components of the CPAM

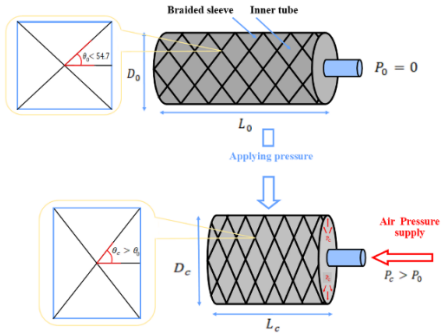

Fig. 3. The structure and operation principle of the CPAM

Where L_0, D_0, and θ_0 are the length, diameter, and angle between the thread of the sleeve and the vertical axis of the CPAM at reset, respectively. After applying air pressure (P_c), the length decreased to L_c, the diameter increased to D_c, and the angle increased to θ_c.

The experiment was performed at pressures ranging from 0 to 250 kPa with an increasing rate of 50 kPa as shown in Fig. 3 and Fig. 4, because the muscle is made of a thin, low-resistance material, which is the balloon, it contracted at a large rate at low pressures, where reached the maximum contraction rate (27.69%), the muscle was length of 14.1 cm, at a pressure of 250 kPa. As for increasing the pressure above 250 kPa, its effect was unclear, and it may also lead to the balloon bursting, therefore the maximum pressure was set to 250 kPa. Fig. 4 illustrates how low pressure affects the muscle, where the muscle constricted at a large rate at 150 kPa, while the impact is much smaller when the pressure is raised to 250 kPa.

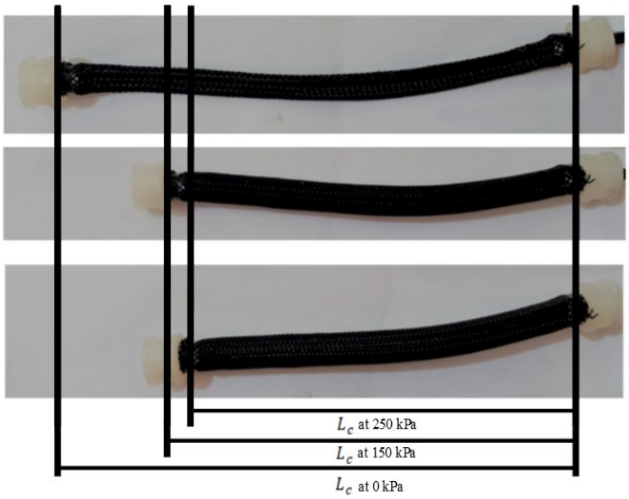

Fig. 4. CPAM at different pressures

Fig. 5 illustrates that CPAM began to contract quickly at a pressure of 50 kPa, and as the pressure increased, the contraction rate increased until it reached 15.1 cm at a pressure of 150 kPa. Beyond this pressure, the contraction decreased until the length reached 14.1 cm at a pressure of 250 kPa.

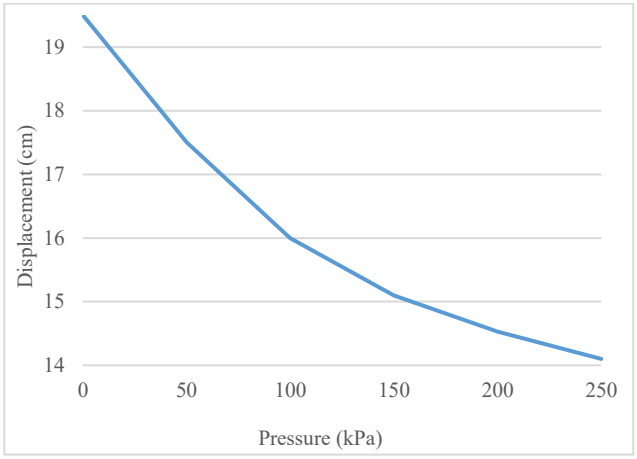

Fig. 5. The correlation between displacement and the pressure in CPAM

III. EXTENSOR PNEUMATIC ARTIFICIAL MUSCLE

The extensor muscle (EPAM) was constructed from a balloon bladder with a length of 15 cm and a sleeve having double the length of the bladder (30 cm) and the same diameter (1 cm), resulting in an angle between the braided thread and the vertical axis greater than 54.7°. The bladder and sleeve ends were connected with 3D-printed ends, exactly like the CPAM. When the muscle was compressed with air, the sleeve expanded with the bladder, causing the diameter of the muscle and the angle to decrease as illustrated in Fig. 6.

The bladder and sleeve for both the CPAM and EPAM are depicted in Fig. 7, where the sleeve's length is double the bladder's length in the EPAM and their diameter is twice that of the sleeve and bladder in the CPAM.

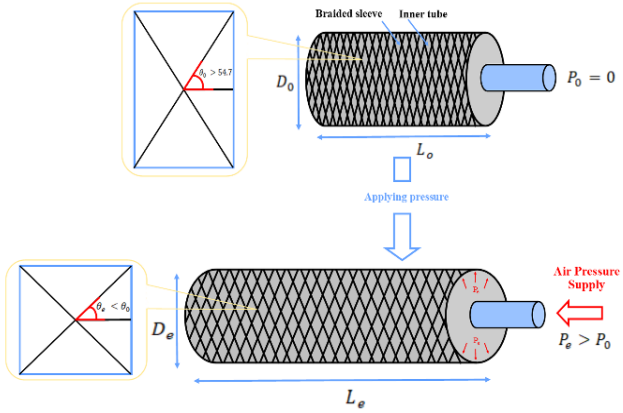

Fig. 6. The structure and operation principle of EPAM

Where L_0, D_0, and θ_0 are the length, diameter, and angle between the thread of the sleeve and the vertical axis of EPAM at reset, respectively (as in CPAM). After applying air pressure (P_e), the length increased to L_e, the diameter decreased to D_e, and the angle decreased to θ_e.

Fig. 7. The difference in the lengths of the bladders and sleeves of both the CPAM and EPAM

Fig. 8 illustrates the extension of the EPAM under various pressures. It depicts the effect of low pressure (150 kPa) on the EPAM, where it expanded significantly. As the pressure increased, the expansion rate continued to increase, reaching 23 cm at 250 kPa, albeit at a slower rate. This deceleration occurred because the EPAM was unable to expand further, as the angle formed between the sleeve's threads approached a value very close to 54.7°.

The experiment was performed under a pressure range from 0 to 250 kPa, as shown in Fig. 9, The pressure was restricted to 250 kPa, because the bladder was made of a balloon, which is a thin material that cannot withstand high pressures, also a good rate of expansion was achieved at this pressure (53.33%).

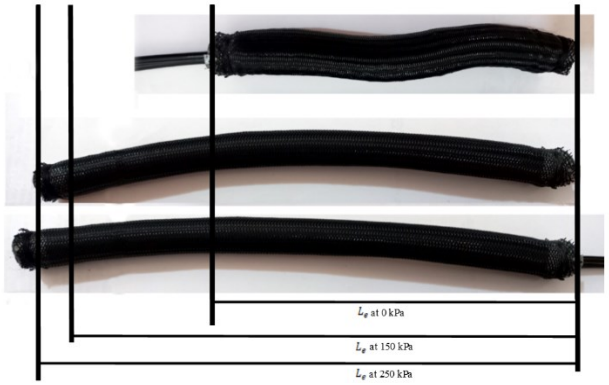

Fig. 8. EPAM at different pressures

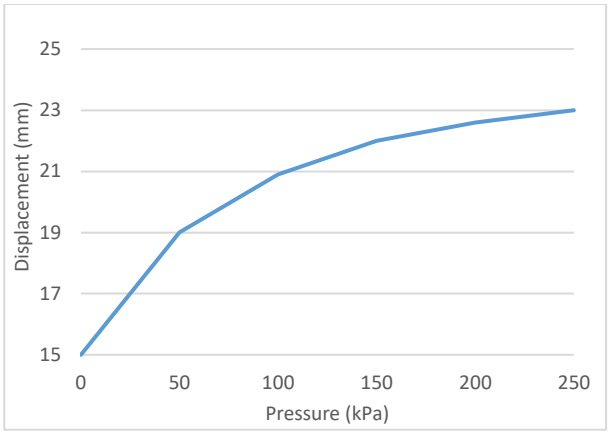

Fig. 9. The correlation between displacement and the pressure in EPAM

IV. EXTENSOR BENDING-PNEUMATIC ARTIFICIAL MUSCLE

The same previous EPAM was sewed with a fixed-length thread on one side to make it EB-PAM, while the other side was left free. When the pressure was applied, the free side expanded (the sleeve is longer than the bladder, so the angle is greater than 54.7°), while the other side did not, because the thread prevented it from expanding, causing the muscle to bend towards the sewed side. The pressure range applied to EB-PAM was 0 to 200 kPa, with an increment of 25 kPa. The angle of bending increases as the applied pressure increases, and because the muscle is made of thin, low-thickness material, it began to bend significantly at low pressure (25 kPa). The bending angle reached its maximum at 200 kPa of pressure, and it remained at this angle even when the pressure on the muscle increased. therefore, the maximum pressure was determined to be 200 kPa.

Fig. 10 and Fig. 11 depict the muscle under various applied pressures. The bending angle was measured from the actuator remote end relative to its initial position, it observed that the bending angle increased significantly at a pressure of 25 kPa, and with a gradual increase in pressure, the angle increased, but at slower rates, until it reached its maximum value (500°) at 200 kPa.

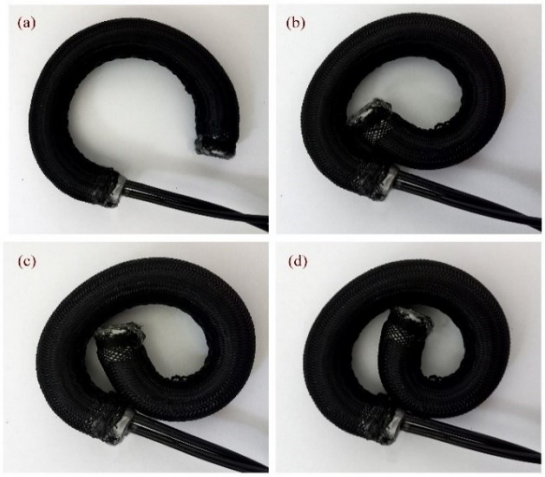

Fig. 10. EB-PAM at different pressures: (a) at 25 kPa, (b) at 75 kPa, (c) at 100 kPa, and (c) at 200 kPa

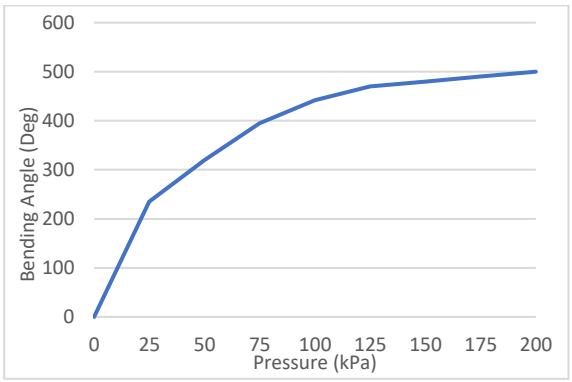

Fig. 11. The bending angle of EB-PAM at different pressure

Three experiments were performed to show muscle stiffness by suspending the muscle from the air-supplying limb on a fixed platform and hanging several weights at the other end. In the first experiment, the bending angle was set to 60°, which was formed at a pressure of 90 kPa. In the second experiment, the bending angle was set to 90° at a pressure of 60 kPa. In the third experiment, the bending angle was 120° at a pressure of 30 kPa. At each experiment, loads from 50g - 200g are applied to the free end of the muscle to determine its stiffness as illustrate in Fig. 12, it was found that the muscle gradually returns to a straight shape with increasing load because of its low stiffness. The stiffness is determined by calculating the change in bending angle at each load.

Fig. 12 and Fig. 13. illustrates how the bending angle changes in response to a load. Although the angle of 60° it has the highest pressure, it has the highest degree of curvature (less stiffness) as shown in Fig. 14. cause this angle has the most portability to deform and the difference in pressure between it and other experiments is very small. Fig. 14. illustrates the low stiffness values of the EB-PAM at angles (60°, 90°, and 120°) where the stiffness range is approximately 300 N/m to less than 450 N/m.

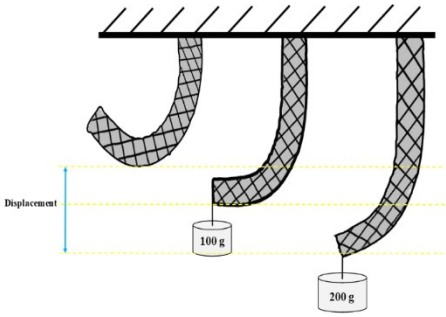

Fig. 12. Schematic overview of stiffness measurement experiment of EB-PAM

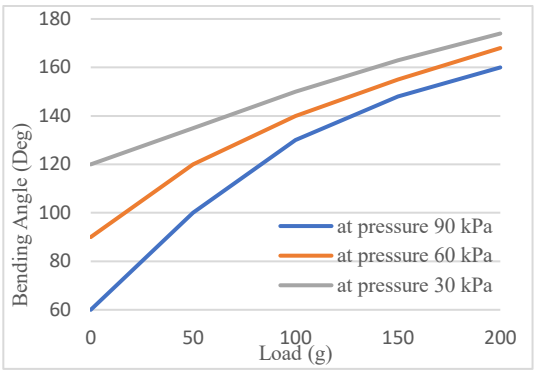

Fig. 13. The bending angle of EB-PAM at different loads

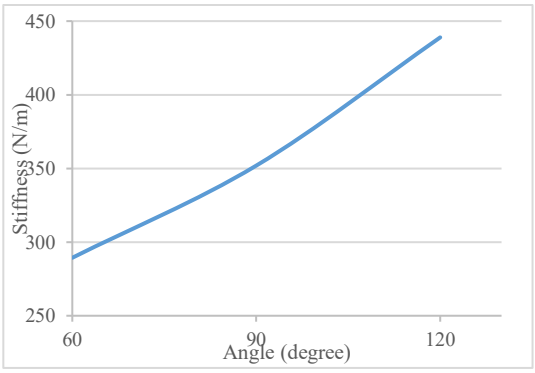

Fig. 14. The stiffness of EB-PAM at bending angles 60°, 90°, and 120°

The EPAM, including EB-PAM, exhibits low stiffness due to its high ability to extend, as illustrated in Table I. With an increase in extension, a corresponding rise in misalignment is observed. Accordingly, a new EB-PAM that has more stiffness was developed by combining the CPAM and EB-PAM, which the following paragraphs will go into more detail about.

TABLE I. DISPLAYS THE CONTRACTION, EXTENSION, AND BENDING VALUES FOR CPAM, EPAM, AND EB-PAM, RESPECTIVELY

Pressure (kPa)	Length of CPAM (cm)	Length of EPAM (cm)	The bending angle of EB-PAM (degree)
0	19.5	15	0
50	17.5	19	320
100	16	20.9	442
150	15	22	480
200	14.5	22.6	500
250	14.1	23	500
Ratio of contraction for CPAM and extension of EPAM	27.69%	53.33%	-

V. NOVEL COMPOUND EXTENSOR BENDING - PNEUMATIC ARTIFICIAL MUSCLE (CEB-PAM)

EPAM, including EB-PAM, is characterized by its high susceptibility to deformation. When the pressure was applied to make it bend at a certain angle, the angle of bending decreased with an increase in the load on it until it returned straight, especially if the muscle is made of thin material. Consequently, the most important characteristic of the new muscle is to keep the bending angle more fixed than EB-PAM under different loads. The new muscle characteristics are as follows:

- Good degree of bendability at low pressures.
- It is more stiffness than EB-PAM.
- At a particular angle, the stiffness can be changed.
- At variable angles, fixed stiffness can be achieved.

VI. DESIGN AND CONSTRUCTION OF THE CEB-PAM

The new muscle is made up of a combination of CPAM and EPAM, where the CPAM placed inside the EPAM. The two muscles were connected by the same endcaps as illustrated in Fig. 15. The design of the muscle began with the construction of two endcaps, one of which is blocked and the other with two holes. One of these holes was in the middle, where the CPAM connected (Fig. 15 (a)), and the other hole was on the side, where the EPAM connected so that air can flow in and out of each muscle.

Fig. 15. Stages of CEB-PAM manufacturing: (a) The endcap design, (b) Connect CPAM to one of the endcaps, (c) CPAM is inserted into the bladder of EPAM, (d) Connect each CPAM and EPAM to the other endcaps and, (e) The actuator was sewn on one side

The CPAM and EPAM were designed having the same dimensions of muscles in the previous paragraphs for both the CPAM and EPAM. The inner bladder was connected to the central part of one endcaps and then inserted into a sleeve that has a similar length of the bladder as illustrated in Fig. 15 (b). The CPAM was inserted into the EPAM bladder (Fig. 15 (c)). It was compressed within the bladder of the EPAM because it is longer (CPAM is longer by 30% than EPAM). The CPAM was then connected to the central part of the other ends, and the bladder of EPAM was connected to the same

ends on both sides. The bladder of the EPAM was inserted with a sleeve that has double the length of the bladder in order to form EPAM (Fig. 15 (d)). The two muscles were tied at both ends with adhesive material and thread. Lastly, to make the muscle bend, one side of the EPAM was sewn with a thread to prevent extending, while the other side was left free as shown in Fig. 15 (e). When the EPAM exposed to 200 kPa of pressure, it bent at an angle of 180° as Fig. 16. because the contraction muscle prevents it from bending further (The angle remains at this value even when the pressure was increased). The angle will gradually decrease as EPAM pressure is reduced and CPAM pressure is increased. Changing these pressures allows for more precise control of the angle.

Fig. 16. The bending angle of CEB-PAM at various pressures for both CPAM and EPAM

VII. STIFFNESS OF THE COMPOUND EXTENSOR-BENDING PNEUMATIC ARTIFICIAL MUSCLE

To test the stiffness of CEB-PAM and compare it to the EB-PAM, the same three experiments were performed at the bending angles (60°, 90°, and 120°), but this time it was possible to control the pressure of both the CPAM and the EB-PAM in forming bending angles at rest (without loads). In other words, the same bending angle can be formed at different pressures for both the CPAM and the EB-PAM.

In the first experiment, the bending angle of CEB-PAM was fixed at 60° (without loads) at pressures of 110 kPa for EB-PAM, then increased the pressure for CPAM to 75 kPa, However, the angle remained at 60°, then different loads were suspended (from 50-200 g), and the bending angles were recorded at each instance. After that, the loads were removed, and then the pressure was increased for both the CPAM and the EB-PAM in a specific proportion until an angle of 60° is formed again at Pe = 180 kPa and Pc= 200 kPa (i.e., the same angle of bending but with different pressures). Then, the loads were suspended, and the corresponding bending angles were recorded. Again, the loads were removed and the pressure was increased for both muscles at Pe = 220 kPa and Pc = 250 kPa to form the angle of 60°. Once more, the loads were resuspended to record their bending angles. The same experiments were repeated at bending angles of 90° and 120° With variations in the applied pressure on each muscle. Fig. 17 shows how the deformation of the angle decreased (i.e., the stiffness increased) as pressure increased for both CPAM and EB-PAM at specific bending angles. There is a noticeable difference between the bending angles between EB-PAM and CEB-PAM. For example, the EB-PAM bending angle reached 160° at load 200 g, after it was 60° without load, whereas the CEB-PAM bending angle reached 116° at the same load.

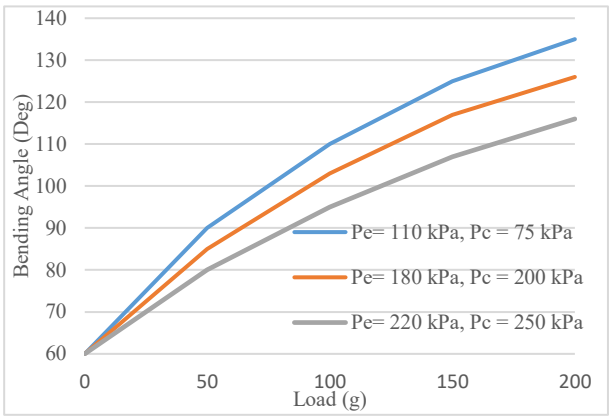

(a)

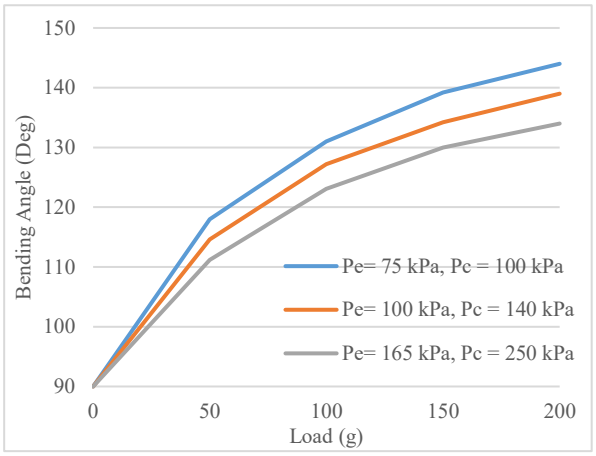

(b)

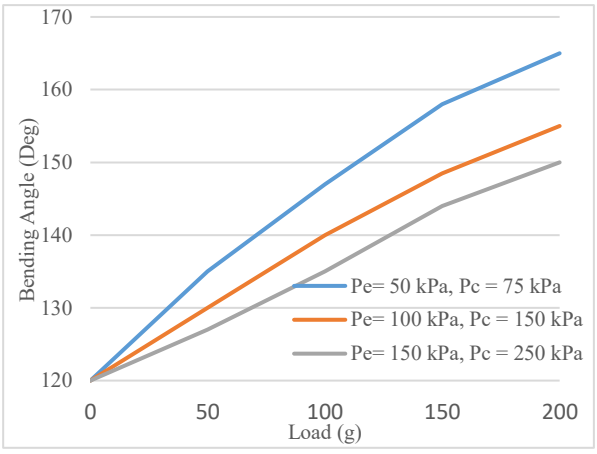

(c)

Fig. 17. The bending angle of CEB-PAM at different loads: (a) at bending angle of 60°, (b) at bending angle of 90°, and (c) at bending angle of 120°.

By calculating the alteration in bending angle under different loads, the stiffness at each of the three angles (60°, 90°, and 120°) can be determined (Fig. 18). The Fig. 18 shows the stiffness increased with an increase in pressure for both CPAM and EB-PAM. The highest stiffness value observed at Pe=220 kPa and Pc=250 kPa at bending angle of 60° (Fig. 18 (a)), while the lowest stiffness value occurred at a bending angle of 120° at Pe=50 kPa and Pc=75 kPa (Fig. 18 (c)). In CEB-PAM, stiffness was significantly increased compared to traditional EB-PAM. While the highest stiffness

value in traditional EB-PAM was less than 450 N/m, stiffness exceeding 850 N/m was achieved with CEB-PAM.

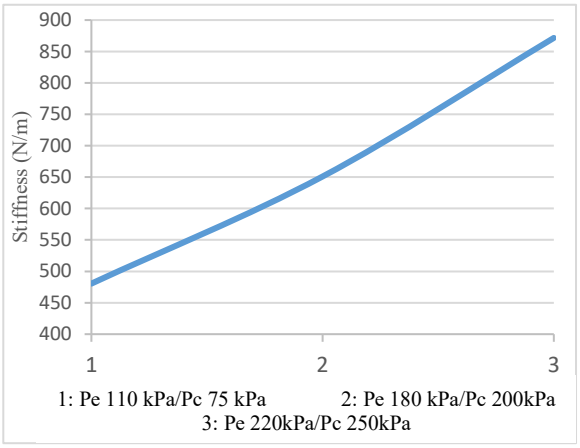

(a)

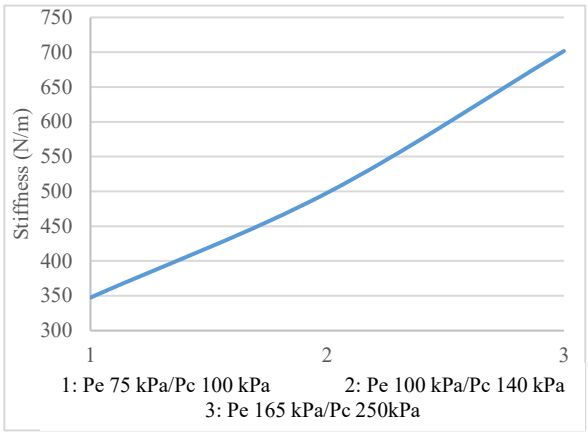

(b)

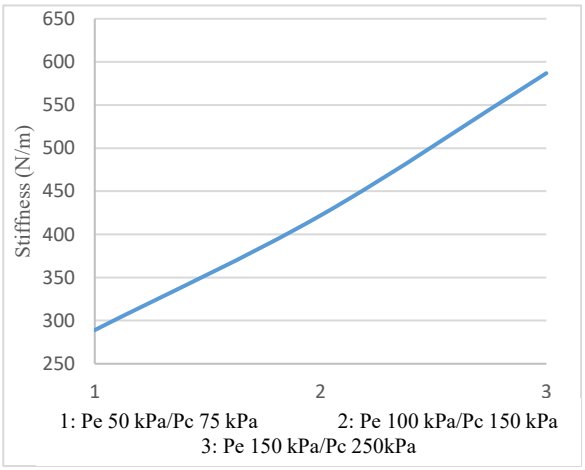

(c)

Fig. 18. The stiffness of CEB-PAM at different angles: (a) at bending angle of 60°, (b) at bending angle of 90°, and (c) at bending angle of 120°

Fig. 18. also illustrates the ability to achieve variable stiffness at a fixed angle. For instance, at a 60° angle, variable stiffness can be attained at 480.447 N/m, 651.028 N/m and 871.562 N/m by changing pressures, and the same as for the other angles. Furthermore, it is possible to achieve a fixed stiffness at different angles. For instance, at a bending angle of 60°, a stiffness of 480 N/m was achieved with Pe=110 kPa, Pc=75 kPa, which is equal to the stiffness at a 90° angle with Pe=100 kPa, Pc=140 kPa.

Due to the balloon material used in manufacturing, the pressure was limited to 250 kPa. However, substituting the balloon with a material capable of withstanding higher pressures would allow for achieving much greater stiffness. As the pressure in the muscle increases, so does the stiffness.

VIII. KINEMATIC ANALYSIS OF THE CEB-PAM

The importance of kinetic analysis is in understanding the performance of PAM and how it interacts with air pressure. This understanding is critical for developing a control model that allows them to execute specific tasks with precision.

The general geometry of the PAM is shown in Fig. 19, assuming that the muscle has a cylindrical shape [71]. As explained previously, L is the muscle length, D is its diameter, and θ is the angle formed by the single thread and the central axis, while n is the number of turns the thread makes around the bladder, and b is its length.

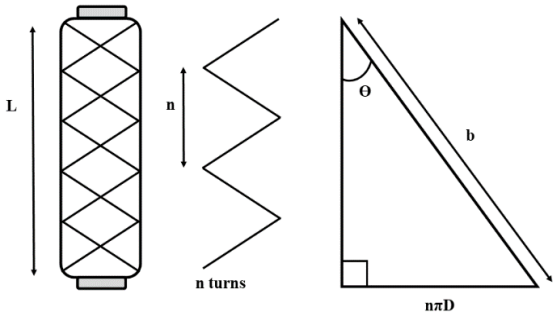

Fig. 19. The general geometry of PAM

Based on general geometry, the following equations are used to calculate L, D, and the volume of the muscle (V):

$$L = b\ \cos\theta \tag{1}$$

$$D = \frac{b \sin\theta}{n\pi} \tag{2}$$

$$V = \frac{\pi D^2 L}{4} \tag{3}$$

EPAM differs from CPAM in that the length of the sleeve is greater than the length of the bladder. In order to equalize the length, EPAM was compressed (as previously explained), i.e., the angle is greater than 54.7°, and as pressure is applied, the angle decreases to reach the lowest energy configuration, causing the muscle to expand. As one side of the EPAM is sewn, this side remained at its maximum angle (θ_{max}), while the angle on the other side, which was free, decreased to θ_e (decreases with increasing pressure), causing the muscle to bend. The CPAM contracts in all directions by the same extent, i.e., the angle increased by the same value (θ_c).

Analysis of the geometrical kinematics of CEB-PAM is illustrated in Fig. 20. The CEB-PAM analysis was based on the assumption that the CPAM maintains its cylindrical shape during a contraction while maintaining the same angle of contraction in all directions, whereas the EPAM maintains a

circular cross-section during extension. Additionally, the thread prevents the muscle from extending on one side; there is no frictional force between the sleeve and the bladder, between the sleeve threads and between CPAM and the bladder of the EPAM; and that there is no elastic force inside the bladder. The length of CPAM (L_c) is 30% longer than EPAM's length (L_e), so the length equation between them is:

$$L_c = 1.3L_e \, , L_e = \frac{1}{1.3} L_c \tag{4}$$

The diameter of EPAM is double that of CPAM, and EPAM sleeve length is double its bladder length. Consequently, the relation between the thread length in CPAM (b_c) and the thread length in EPAM (b_e) is represented by the equation:

$$2\, b_c \; = \; 1.3\, b_e \, , b_e \, = \; \frac{2}{1.3} \; b_c \tag{5}$$

The relation between the number of turns in CPAM (n_c) and the number of turns in EPAM (n_e) is represented by the equation:

$$n_c = 1.3\, n_e \, , n_e \, = \frac{1}{1.3} \; n_c \tag{6}$$

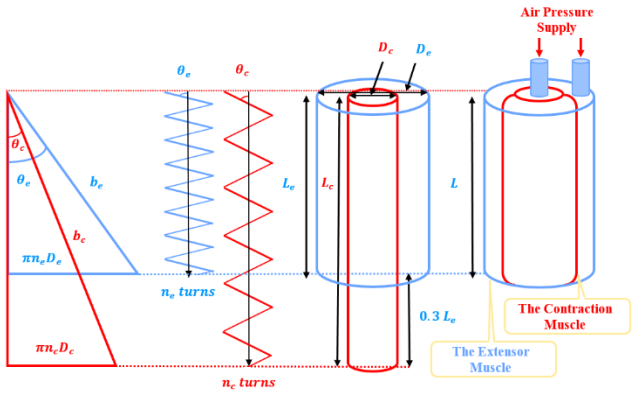

Fig. 20. Kinematics of the CEB-PAM: (a) The general geometry of the CPAM and EPAM that make up the CEB-PAM, (b) The braid angles and the number of turns of the two muscles, (c) Relation between muscle lengths and, (c) The design of CEB-PAM

Based on Fig. 19, The geometric parameters for CPAM (CPAM remains cylindrical inside EPAM):

$$L_c = \; b_c \cos \theta_c \tag{7}$$

$$D_c = \frac{b_c \sin \theta_c}{\pi n_c} \tag{8}$$

$$V_c = \frac{\pi {D_c}^2 L_c}{4} \tag{9}$$

Where V_c is the volume of CPAM.

The geometric model of EB-PAM is shown in Fig. 21, where L_n is the muscle length on the free side, L_o is the muscle length on the reinforced side, and α is the muscle's bend angle.

$$L_e = \frac{L_o + L_n}{2} \tag{10}$$

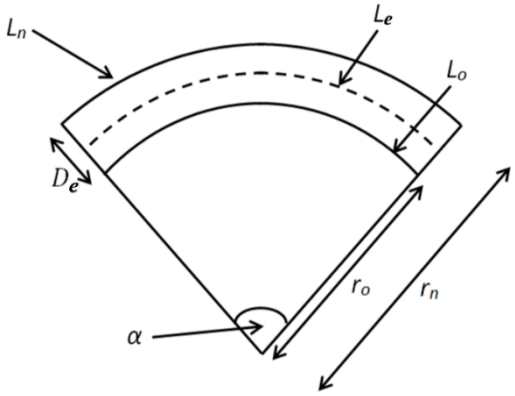

Fig. 21. The geometry of EB-PAM

About the inner and outer radiuses, the muscle diameter (D_e) is calculated by:

$$D_e = r_n - r_o \tag{11}$$

Where r_o is the inner radius, and r_n is the outer radius.

L_n and L_o are calculated by combining Equation (1) and the arc length:

$$L_o = b_e \cos \theta_{max} \; = \; r_o \alpha \tag{12}$$

$$L_n = b_e \cos \theta_e \; = \; r_n \alpha \tag{13}$$

As explained previously, the angle of the braid is unequal on the two sides. That is because when the pressure inside the muscle increases, the bending increased as a result of a decrease in the angle of the braid at the outside edge (point A) to θ_{max} (point B) in Fig. 22. So, each angle will have an associated muscle diameter. Assuming that the muscle cross-section is perfectly circular, the overall diameter will be the sum of the radiuses on the outside (r1) and inside (r2) of the curve as shown in Fig. 22. The diameter of the bent muscle can be calculated from equation (2):

$$r_1 = \frac{D_1}{2} = \frac{b_e \; \sin \theta_e}{2\pi n_e} \tag{14}$$

$$r_2 = \frac{D_2}{2} = \frac{b_e \; \sin \theta_{max}}{2\pi n_e} \tag{15}$$

$$D_e = r_1 + r_2 \tag{16}$$

$$D_e = \frac{b_e \; \sin \theta_e \; + \; b_e \; \sin \theta_{max}}{2\pi n_e} \tag{17}$$

The kinematic equations for the EB-PAM can be developed to describe the bending angle (α), the radius of curvature (r_o), and the length of the muscle central axis (L_e). Equation (11) is substituted for equation (13) and then equation (12) is substituted we get (18).

$$L_n = \left(D_e + \frac{L_o}{\alpha}\right)\alpha = D_e\,\alpha + L_o = b_e\,\cos\theta_e \tag{18}$$

Equations (12) and (18) can be used to drive α as a function of θ_e and θ_{max} using the following equation:

$$\alpha = \frac{b_e\,\cos\theta_e\, - b_e\,\cos\theta_{max}}{D_e} \tag{19}$$

The muscle length was determined by substituting Equations (12) and (13) in Equation (10):

$$L_e = \frac{b_e\,cos\theta_{max} + b_e\,cos\theta_e}{2} \tag{20}$$

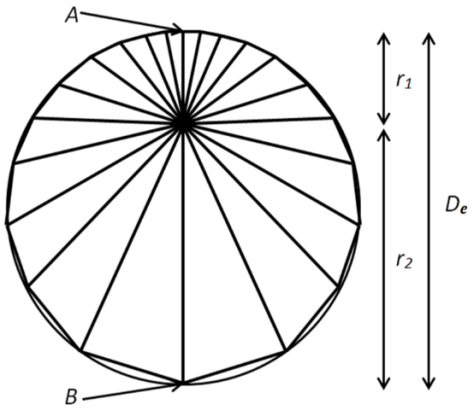

Fig. 22. Radius inside the curved muscle

IX. MODELING THE OUTPUT FORCE OF THE CEB-PAM

The force of CEB-PAM was mathematically calculated using Chou's theory of energy conservation [71], which assumes that the input work is equal to the output work. In this framework, the applied pressure and volume change represent as the actuator's input work, while the force and change in muscle length represent the actuator's output work. By substituting the kinetic analysis equations into the volume, which is assumed to be cylindrical, a force equation can be derived.

$$dW_{in} = dW_{out} \tag{21}$$

The input work (W_{in}) is represented by applied air pressure which acts on the inner surface of the muscle and causes a change in muscle volume:

$$dW_{in} = P.dV \tag{22}$$

Where P is the relative differential air pressure which is equal to P_e in EB-PAM and equal to $P_c - P_e$ in CPAM. While the output work (W_{out}), is associated with an increase in the actuator length or bend (L) as a result of the size change:

$$dW_{out} = F.dL \tag{23}$$

Therefore, by combining equations (22) and (23), the output force (F) can be calculated as (24).

$$F = P\frac{dV}{dL} \tag{24}$$

Based on the volume of a cylinder in equation (9), and by substituting the equations (17) and (20) in equation volume, The curved muscle volume (V_e) will be:

$$V_e = \frac{\pi D_e{}^2 L_e}{4} = \frac{b_e{}^3(\cos\theta_e + \cos\theta_{max})(\sin^2\theta_e + 2\sin\theta_{max}\sin\theta_e + \sin^2\theta_{max})}{32\pi n_e{}^2} \tag{25}$$

And by substituting equations (7) and (8) in equation (9), the volume of CPAM will be:

$$V_c = \frac{b_c^3\,sin^2\theta_c\,cos\theta_c}{4\,\pi n_c^2} \tag{26}$$

Differentiating equations (7) and (26) with respect to θ_c, and differentiating equations (20) and (25) with respect to θ_e gives:

$$\frac{dL_c}{d\theta_c} = -b_c sin\theta_c \tag{27}$$

$$\frac{dV_c}{d\theta_c} = \frac{b_c^3\,sin\theta_c}{4\,\pi n_c^2} = (\,3\,cos^2\theta_c\, -\, 1) \tag{28}$$

$$\frac{dL_e}{d\theta_e} = \frac{-bsin\theta_e}{2} \tag{29}$$

$$\frac{dV_e}{d\theta_e} = \frac{b_e{}^3}{32\pi n_e{}^2}\,((\cos\theta_e + \cos\theta_{max})(2\cos\theta_e\sin\theta_e + 2\sin\theta_{max}\cos\theta_e) - \sin\theta_e\,(\sin\theta_e + \sin\theta_{max})^2) \tag{30}$$

Equations (27) and (28) can be substituted for equation (24) to produce the following mathematical model of the proposed CPAM output force:

$$F_c = \frac{b_c^2\,(P_c - P_e)}{4\pi n_c^2}(3\cos^2\theta_c - 1) \tag{31}$$

It is important to note that the muscle or cylinder volume refers to the volume of compressed air inside it. Thus, in the case of the EB-PAM, the cylindrical EB-PAM volume (V_s) is the difference between EB-PAM volume and CPAM volume. This is because CPAM takes space inside the EB-PAM in a volume. As a result, the force in EB-PAM (F_e) will be:

$$F_e = P_e\frac{dV_s}{dL_e} = P_e\frac{dV_e - dV_c}{dL_e} = P_e\left(\frac{dV_e}{dL_e} - \frac{dV_c}{dL_e}\right) = P_e\left(\frac{dV_e}{dL_e} - 1.3\frac{dV_c}{dL_c}\right) \tag{32}$$

By substituting equations (27), (28), (29), and (30) in equation (32):

$$F_e = P_e \frac{b_e^2}{4\,\pi n_e^2}\left(0.325\,(3cos^2\,\theta_c - 1) - \left(\frac{(\cos\theta_e + \cos\theta_{max})(\sin\theta_e\cos\theta_e + \sin\theta_{max}\cos\theta_e)}{2sin\theta_e} - \frac{(\sin\theta_e + \sin\theta_{max})^2}{4}\right)\right) \quad (33)$$

The resulting force of the CEB-PAM is the difference between the EB-PAM force (F_e) and CPAM force (F_c):

$$F = (F_c - F_e) \quad (34)$$

By substituting into the force equations for both CPAM and EB-PAM at specific pressures and substituting it into the last equation, the bending force of the CEB-PAM is calculated mathematically, and to verify the validity of the results of the mathematical model, the force was calculated experimentally.

X. Verification Of The CEB-PAM Output Force Modeled By Experimentation

This CEB-PAM output force mathematical model was validated by placing it in a rig that held it in an isometric configuration at a range of known bending angles as shown in Fig. 23. A load cell was attached to the muscle remote end, allowing actuator force to be measured and recorded to a computer.

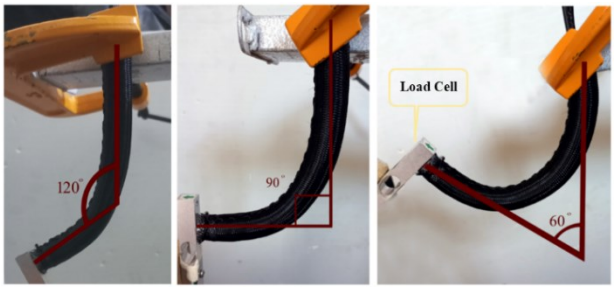

Fig. 23. A test rig is used to measure muscle force at various bending angles

To test the muscle, it was placed in the rig and then the pressure was applied to CPAM and EB-PAM. The experiment was repeated at muscle bend angles of 60°, 90°, and 120°, with three experiments performed at each angle to measure the force of the CEB-PAM. In each experiment, the pressure on the CPAM was increased from 0 to 250 kPa while the pressure on the EB-PAM remained fixed as shown in Fig. 24, Fig. 25, and Fig. 26. In the first, second and third experiments, the pressure of EB-PAM was 100 kPa, 150 kPa, and 250 kPa, respectively. Fig. 24, Fig. 25, and Fig. 26 illustrate the results of these experiments (at the specified angles) and their comparison to those obtained mathematically. It also illustrates that the bending force decreases as the pressure increases in the CPAM muscle, at a fixed pressure for the EB-PAM. The average error percentages between experimental and mathematical results at the bending angle of 60° were 22.35 % at P_e= 100 kPa, 22.56 % at P_e = 150 kPa and, 23.14 % at P_e= 250 kPa. At the bending angle of 90° the average error percentages were 21.93%, 22.02%, and 21.38% at P_e = 100 kPa, 150 kPa, and 250 kPa respectively. At the bending of angle 120° the average error percentages were 21.5%, 21.39%, and 22.19%, respectively.

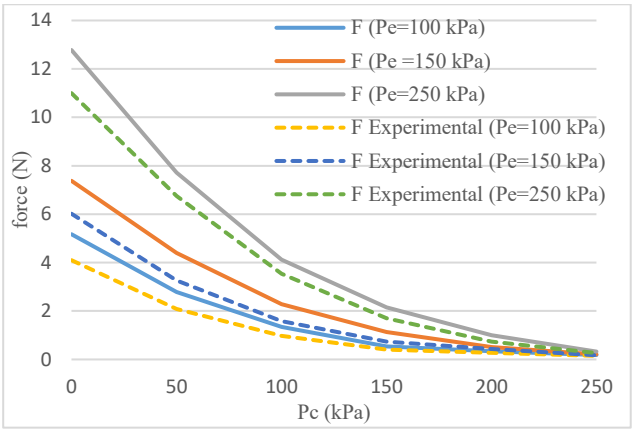

Fig. 24. Experimental and mathematical results of the output force of CEB-PAM at the angle of 60°

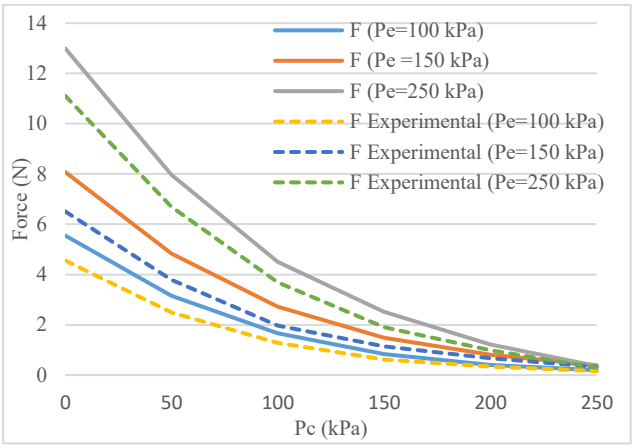

Fig. 25. Experimental and mathematical results of the output force of CEB-PAM at the angle of 90°

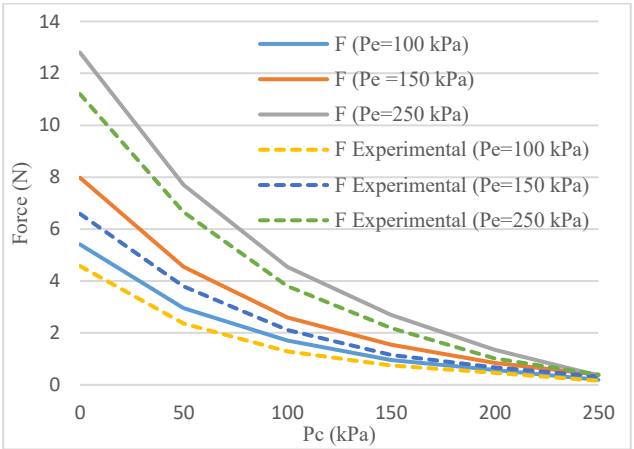

Fig. 26. Experimental and mathematical results of the output force of CEB-PAM at the angle of 120°

XI. ENHANCEMENT TO THE MATHEMATICAL MODEL BASED ON RADIAL EXPANSION PRESSURE

One of the factors that contribute to muscle energy loss is that the bladder needs the energy to expand radially until it contacts the braided sleeve. In other words, the force will be equal to zero at the pressure required by the muscle for the bladder to expand to contact with the sleeve [72][73]. Therefore, in the CEB-PAM, each of the CPAM and EB-PAM will lose energy to contact the bladder with the sleeve as shown in Fig. 27.

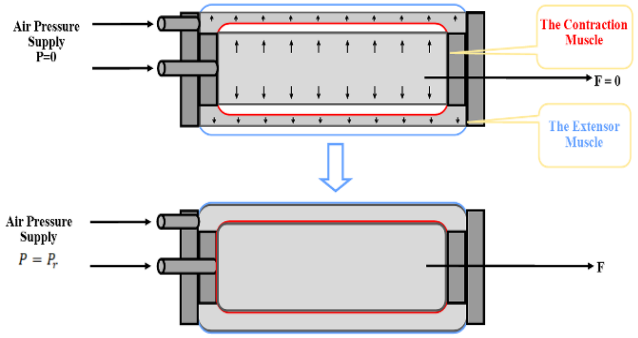

Fig. 27. The pressure required by CPAM and EB-PAM to contact the bladder with the sleeve

If the pressure required to expand the bladder is P_r, the actual pressure (P_a) will be as follows:

$$P_a = P - P_r \tag{35}$$

The actual pressure for each CPAM and EB-PAM was calculated using Tsagarakis and Caldwell's pressure model for radial expansion, which is expressed by the following equation:

$$P_r = K_r(D_o - D_c \sin\theta_c) \tag{36}$$

$$K_r = 2000\frac{kPa}{m} \; for \; D_c \sin\theta < \frac{D_o}{2} \tag{37}$$

$$K_r = 500 \; \frac{kPa}{m} \; for \; D_c \sin\theta > \frac{D_o}{2} \tag{38}$$

Where D_o is the actual diameter of the muscle and K_r is the elasticity of the linearized radial actuator [73]. From equation (36), CPAM and EB-PAM radial pressure is represented by the following equation:

$$P_{re} = K_r(D_{oe} - D_e \sin\theta_e) \tag{39}$$

$$P_{rc} = K_r(D_{oc} - D_c \sin\theta_c) \tag{40}$$

Where D_{oe} and D_{oc} are the actual diameters of EB-PAM and CPAM respectively. As such, the actual pressure of each ECPAM and CPAM will be:

$$P_{ae} = P_e - P_{re} \tag{41}$$

$$P_{ac} = P_c - P_{rc} \tag{42}$$

Substitution equation (41) in equation (33), the EPAM force equation will be:

$$F_e = P_{ae}\frac{b_e^2}{4\,\pi n_e^2}\left((0.325\,(\,3\,cos^2\theta_c - 1) - \left(\frac{(\cos\theta_e + \cos\theta_{max})(\sin\theta_e\cos\theta_e + \sin\theta_{max}\cos\theta_e)}{2sin\theta_e} - \frac{(\sin\theta_e + \sin\theta_{max})^2}{4}\right)\right) \tag{43}$$

And substitution equations (41) and (42) in equation (31), the CPAM force equation will be:

$$F_c = \frac{b_c^2\,(P_{ac} - P_{ae})}{4\pi n_c^2}(3\cos^2\theta_c - 1) \tag{44}$$

The graphs in Fig. 28, Fig. 29, and Fig. 30 show that when using this enhancement, the difference between the mathematical and experimental results is reduced. Hence the average percentage errors are reduced too, which equals to 8.81%, 8.95%, and 9.39% at a bending angle of 60°; 8.63%, 9.1%, and 8.34% at a bending angle of 90°; 8.28%, 8.37%, and 8.55% at a bending angle of 120° at P_e= 100 kPa, 150 kPa, and 250 kPa respectively.

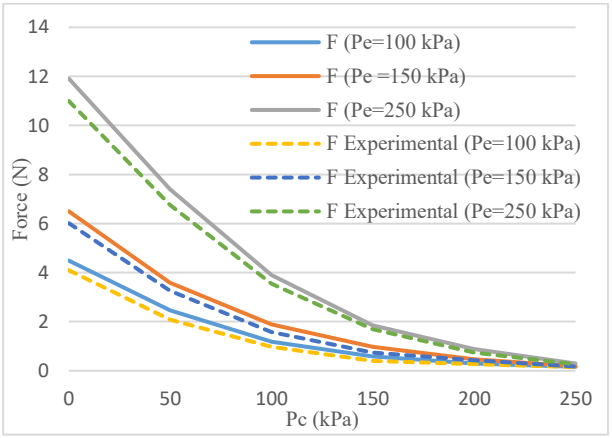

Fig. 28. Output force of the CEB-PAM with P_r at the angle of 60°

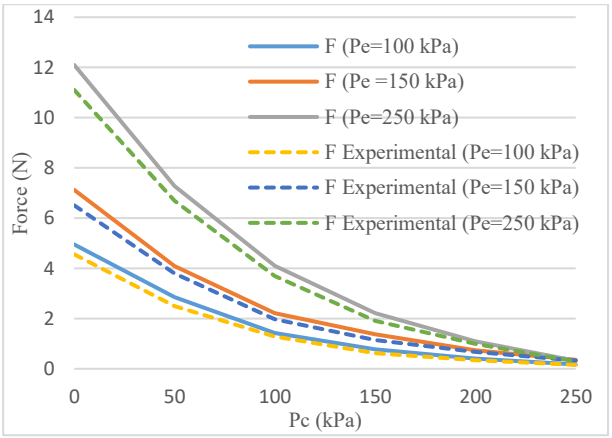

Fig. 29. Output force of the CEB-PAM with P_r at the angle of 90°

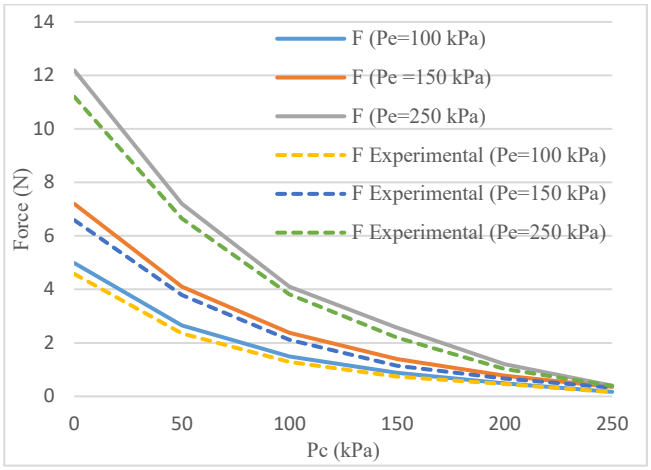

Fig. 30. Output force of the CEB-PAM with P_r at the angle of 120°

XII. Enhancement to the Mathematical Model Based on the Actual Diameter

To further enhance the mathematical model and reduce the average error between the experimental and mathematical results, the thickness of each bladder (t_b) and the sleeve (t_s) were calculated. As previously explained, the volume in the force equation represents the volume of compressed air inside the muscle, not the volume of the muscle. Accordingly, the thickness affects the volume and thus the force of the muscle. In the previous calculations, the muscle volume was calculated (the thickness within the volume). In this enhancement, the air volume was calculated by subtracting the thickness of the sleeve and the bladder for each CPAM and EB-PAM from the muscle diameters equations. So the diameters equations for CPAM and EB-PAM will be as follows:

$$D_{ae} = D_e - 2t_a = \frac{b_e \sin\theta_e + b_e \sin\theta_{max}}{2\pi n_e} - 2t_a \tag{45}$$

$$D_{ac} = D_c - 2t_a = \frac{b_c \sin\theta_c}{\pi n_c} - 2t_a \tag{46}$$

$$t_a = t_s + t_b \tag{47}$$

Where D_{ae} is the actual diameter of EB-PAM, and D_{ac} is the actual diameter of CPAM. And because the two muscles are made of the same bladder and sleeve, their thickness is the same.

The actual volume of EB-PAM (V_{ae}) will be:

$$V_{ae} = \frac{\pi {D_a}^2 L_e}{4} = \frac{1}{32\,{n_e}^2\,\pi}\,((b_e \cos\theta_{max} + b_e \cos\theta_e)\,((b_e \sin\theta_e + b_e \sin\theta_{max}) - 4\,n_e\,\pi\,t_a)^2) \tag{48}$$

Differentiating the actual volume of EB-PAM with respect to θ_e gives (49).

$$\frac{dV_{ae}}{d\theta_e} = \frac{1}{32{n_e}^2\pi}\,(2{b_e}^2 \cos\theta_e\,(\cos\theta_e + \cos\theta_{max})\,(b_e(\sin\theta_e + \sin\theta_{max}) - 4\pi n_e t_a) - b_e \sin\theta_e\,(b_e(\sin\theta_e + \sin\theta_{max}) - 4\pi n_e t_a)^2) \tag{49}$$

The EB-PAM force can thus be calculated using equation (32) as follows:

$$F_e = P_{ae}\left(\frac{dV_{ae}}{dL_e} - 1.3\frac{dV_c}{dL_c}\right) \tag{50}$$

By substitution equations (27), (28), (29), and (49) in equation (50), the force of EPAM will be:

$$F_e = \frac{P_{ae}}{4\pi n_e^2}\,[0.325\,b_e^2(3cos^2\theta_c - 1) - \frac{1}{4b_e \sin\theta}\,(2{b_e}^2 \cos\theta_e\,(\cos\theta_e + \cos\theta_{max})(b_e(\sin\theta_e + \sin\theta_{max})\,4\pi n_e t_a) - b_e \sin\theta_e\,(b_e(\sin\theta_e + \sin\theta_{max}) - 4\pi n_e t_a)^2)] \tag{51}$$

Similarly, the actual volume of CPAM (V_{ac}) will be:

$$V_{ac} = \frac{\pi {D_{ac}}^2 L_c}{4} = \frac{\pi b_c \cos\theta_c}{4}\left(\frac{b_c^2 \sin^2\theta_c}{\pi^2 n_c^2} - \frac{4\,t_a b_c \sin\theta_c}{\pi n_c} + 4t_a^2\right) \tag{52}$$

Differentiating the actual volume of CPAM with respect to θ_c:

$$\frac{dV_{ac}}{d\theta_c} = \frac{b_c^3}{4\pi n_c^2}\sin\theta_c(3cos^2\theta_c - 1) - \frac{b_c^2\,t_a}{n_c}(2cos^2\theta_c - 1) - \pi b_c t_a^2 \sin\theta_c \tag{53}$$

By using equation (24), the force of CPAM will be:

$$F_c = -(P_{ac} - P_{ae})\frac{dV_{ac}}{dL_c} \tag{54}$$

And by substitution equations (27) and (53) in equation (54), the CPAM's force will be:

$$F_c = -(P_{ac} - P_{ae})\,[\frac{b_c\,t_a}{n_c \sin\theta_c}\,(2cos^2\theta_c - 1) - \frac{b_c^2}{4\pi n_c^2}(3cos^2\theta_c - 1) + \pi t_a^2] \tag{55}$$

The average percentage error across the three bending angles were 6.44%, 6.72%, and 7.12% at the bending angle of 60°; 6.11%, 6.64%, and 5.98% at the angle of 90°; 6.08%, 6.31%, and 6.48% at the angle of 120°, at P_e= 100 kPa, 150 kPa, and 250 kPa respectively. Fig. 31, Fig. 32, and Fig. 33

illustrate the results obtained after this enhancement in comparison with the experimental result.

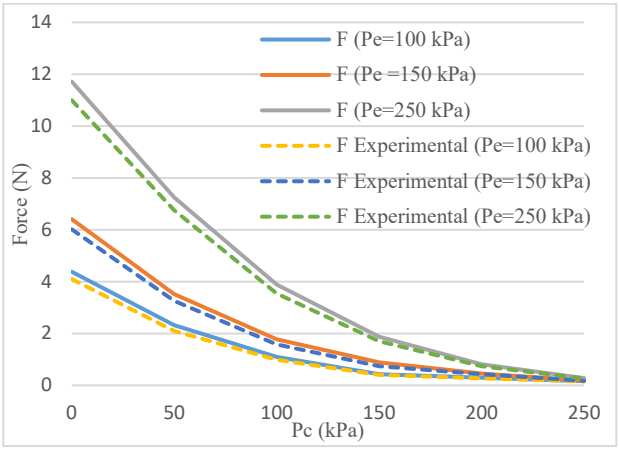

Fig. 31. The force of the CEB-PAM with t_a at the angle of 60°

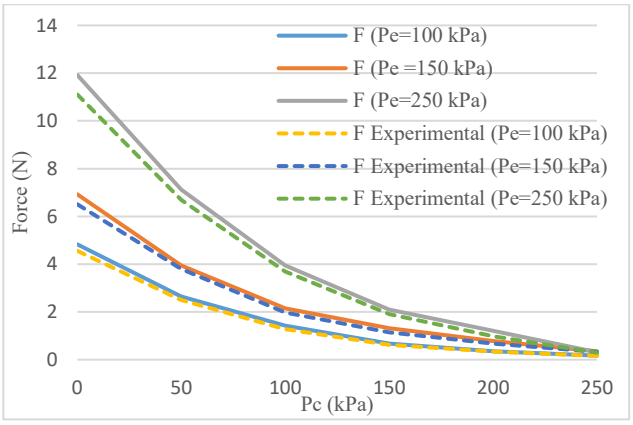

Fig. 32. The force of the CEB-PAM with t_a at the angle of 90°

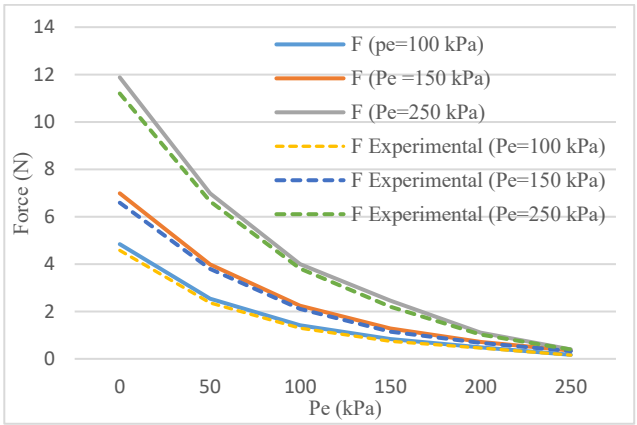

Fig. 33. The force of the CEB-PAM with t_a at the angle of 120°

XIII. CONCLUSION

Enhancing the stiffness of soft robots not only improves their stability during operations but also expands their applicability to tasks demanding precision and interaction with the environment. The ability to control stiffness enhances the robot's flexibility and adaptability, ultimately increasing its effectiveness and safety in various applications.

This paper presents a new muscle made of lightweight balloons that can bend at a high rate under low pressure, combining CPAM and EB-PAM. The new muscle, CEB-PAM, is distinguished by its higher stiffness than Traditional EB-PAM, its ability to change its stiffness at a specific angle, and it is also possible to obtain constant stiffness at different angles

To comprehend the dynamic behavior of the muscle and develop more effective and accurate control strategies. A mathematical model was developed to calculate the output force of CEB-PAM in order to validate this model. Experiments were performed with three different bending angles (60°, 90°, and 120°), with three other experiments were performed with different pressures for each angle. The results of the mathematical model were compared with the experimental results, and the average error between them was more than 20% in all experiments. To improve the mathematical model and reduce the difference in results, the wasted energy consumed by the actuator was calculated before the actual start of expanding or bending (the energy required for the bladder to expand and contact the sleeve), and the thickness of the bladder and sleeve were also calculated to improve the mathematical model even further. The average error was reduced to 7% in all experiments after enhancements.

While employing balloons in manufacturing facilitated the production of a lightweight and cost-effective model that performs adequately under low pressures, the thin material of the balloon diminishes its efficiency. The response to air pressures becomes irregular, and the model is more susceptible to environmental factors like temperature and humidity. These variables have contributed to the emergence of an error rate between the mathematical model and the experimental model. Furthermore, the omission of friction calculations between the bladder and the sleeve for each muscle, as well as between the sleeve threads and the bladder in CEB-PAM and CPAM, contributed to the observed average error.

In future work, this friction force can be calculated and a control model for the operator can be created using this mathematical model to create a lightweight and cheap robot. It works with high accuracy at low pressures. It can be used in several fields, such as industrial and medical fields, which enable it to interact with humans more safely.

REFERENCES

[1] B. Jamil, H. Rodrigue, and Y. Choi, "Design of a novel sensing method for a pneumatic artificial muscle actuator-driven 2-Degrees of freedom parallel joint," *Soft Robotics*, vol. 10, no. 1, pp. 187-196, 2023, doi: 10.1089/soro.2021.0097

[2] Q. Xie, T. Wang, S. Yao, Z. Zhu, N. Tan, and S. Zhu, "Design and modeling of a hydraulic soft actuator with three degrees of freedom," *Smart Materials and Structures*, vol. 29, no. 12, p. 125017, 2020, doi: 10.1088/1361-665X/abc26e

[3] F. Daerden and D. Lefeber, "Pneumatic artificial muscles: actuators for robotics and automation," *European journal of mechanical and environmental engineering*, vol. 47, no. 1, pp. 11-21, 2002.

[4] D. Al-Shamkhani, F. Al-Farhan, and A. Al-Ibadi, "The wearable foot rehabilitation soft robot," In *2021 International Conference on Communication & Information Technology (ICICT)*, pp. 197-201, 2021, doi: 10.1109/ICICT52195.2021.9568432.

[5] A. Al-Ibadi, K. A. Abbas, M. Al-Atwani, and H. Al-Fahaam, "Design, Implementation, and Kinematics of a Twisting Robot Continuum Arm Inspired by Human Forearm Movements," *Robotics*, vol. 11, no. 3, p. 55, 2022, doi: 10.3390/robotics11030055.

[6] A. Al-Ibadi, "The Design and Implementation of a Single-Actuator Soft Robot Arm for Lower Back Pain Reduction," *Iraqi J. Electr. Electron. Eng.*, 2020, doi: 10.37917/ijeee.sceeer.3rd.

[7] B. Yu, J. Yang, R. Du, and Y. Zhong, "A versatile pneumatic actuator based on scissor mechanisms: Design, modeling, and experiments," *IEEE Robotics and Automation Letters*, vol. 6, no. 2, pp. 1288-1295, 2021, doi: 10.1109/LRA.2021.3057286

[8] A.-F. Hassanin, D. Steve, and N.-M. Samia, "A novel, soft, bending actuator for use in power assist and rehabilitation exoskeletons," In *2017 IEEE/RSJ International Conference on Intelligent Robots and Systems (IROS)*, pp. 533-538, 2017, doi: 10.1109/IROS.2017.8202204

[9] L. Hines, K. Petersen, G. Z. Lum, and M. Sitti, "Soft actuators for small-scale robotics," *Advanced materials*, vol. 29, no. 13, p. 1603483, 2017, doi: 10.1002/adma.201603483.

[10] X. Chen, S. Zhang, K. Cao, C. Wei, W. Zhao, and J. Yao, "Development of a wearable upper limb rehabilitation robot based on reinforced soft pneumatic actuators," *Chinese Journal of Mechanical Engineering*, vol. 35, no. 1, p. 83, 2022, doi: 10.1186/s10033-022-00749-6.

[11] A.-R. Ziad, M. Al-Ibadi, and A. Al-Ibadi, "Design and Implementation of a Multiple DoF Soft Robot Arm Using Exestensor Muscles," In *2022 9th International Conference on Electrical and Electronics Engineering (ICEEE)*, pp. 170-174, 2022, doi: 10.1109/ICEEE55327.2022.9772525.

[12] X. Zhu and B. He, "Underactuated rehabilitation robotics for hand function," *Journal of Robotics and Control (JRC)*, vol. 2, no. 5, pp. 337-341, 2021, doi: 10.18196/jrc.25103.

[13] S. A. Al-Ibadi, L. A. T. Al Abeach, and M. A. A. Al-Ibadi, "Soft Robots: Implementation, Modeling, and Methods of control," *Indonesian Journal of Electrical Engineering and Informatics (IJEEI)*, vol. 11, no. 1, pp. 194-209, 2023, doi: 10.52549/ijeei.v11i1.4288

[14] Q. Guan, J. Sun, Y. Liu, and J. Leng, "A bending actuator based on extensile PAM and its applications for soft robotics," In *Proceedings of the 21st International Conference on Composite Materials*, pp. 20-25, 2017.

[15] A. Alipour, M. J. Mahjoob, Z. Fakhari, and A. Nazarian, "A New 4-DOF Robot for Rehabilitation of Knee and Ankle-Foot Complex: Simulation and Experiment," *arXiv preprint arXiv:2011.04230*, 2020, doi: 10.18196/jrc.v3i4.14759.

[16] A. S. Ahmed and S. K. Kadhim, "A Comparative Study Between Convolution and Optimal Backstepping Controller for Single Arm Pneumatic Artificial Muscles," *Journal of Robotics and Control (JRC)*, vol. 3, no. 6, pp. 769-778, 2022, doi: 10.18196/jrc.v3i6.16064.

[17] A. U. Nisa, S. Samo, R. A. Nizamani, A. Irfan, Z. Anjum, and L. Kumar, "Design and Implementation of Force Sensation and Feedback Systems for Telepresence Robotic Arm," *Journal of Robotics and Control (JRC)*, vol. 3, no. 5, pp. 710-715, 2022, doi: 10.18196/jrc.v3i5.15959

[18] A. A. Abed, A. Al-Ibadi, and I. A. Abed, "Vision-Based Soft Mobile Robot Inspired by Silkworm Body and Movement Behavior," *Journal of Robotics and Control (JRC)*, vol. 4, no. 3, pp. 299-307, 2023, doi: 10.18196/jrc.v4i3.16622.

[19] H. A. Al-Mosawi, A. Al-Ibadi, and T. Y. Abdalla, "An Adaptive Parallel Fuzzy And Proportional Integral Controller (APFPIC) For The Contractor Pneumatic Muscle Actuator Position Control," In *2022 International Conference on Electrical, Computer, Communications and Mechatronics Engineering (ICECCME)*, pp. 1-6, 2022, doi: 10.1109/ICECCME55909.2022.9987972.

[20] S. Zhong *et al.*, "A contraction length feedback method for the McKibben pneumatic artificial muscle," *Sensors and Actuators A: Physical*, vol. 334, p. 113321, 2022, doi: 10.1016/j.sna.2021.113321.

[21] S. Udhayakumar, R. Bharath, N. Kowshik Santhakumar, and B. Mohamed Samsudeen Soofi, "Review on Applications of Pneumatic Air Muscle," in *Advances in Forming, Machining and Automation: Select Proceedings of AIMTDR 2021: Springer*, pp. 655-666, 2022, doi: 10.1007/978-981-19-3866-5_52.

[22] N. S. Shalal and W. S. Aboud, "Smart robotic exoskeleton: A 3-dof for wrist-forearm rehabilitation," *Journal of Robotics and Control (JRC)*, vol. 2, no. 6, pp. 476-483, 2021, , doi: 10.18196/jrc.26125.

[23] D. Dragone *et al.*, "Design, computational modelling and experimental characterization of bistable hybrid soft actuators for a controllable-compliance joint of an exoskeleton rehabilitation robot," In *Actuators*, vol. 11, no. 2, p. 32, 2022, doi: 10.3390/act11020032

[24] A. Al-Ibadi, S. Nefti-Meziani, and S. Davis, "Novel models for the extension pneumatic muscle actuator performances," in *2017 23rd international conference on automation and computing (ICAC)*, pp. 1-6, 2017, doi: 10.23919/IConAC.2017.8081973.

[25] L. Margheri and B. Trimmer, "Soft robotics community events: Meeting different backgrounds for common challenges," *Soft Robotics*, vol. 1, no. 4, pp. 236-238, 2014, doi: 10.1089/soro.2014.1505

[26] H. Al-Fahaam, S. Davis, and S. Nefti-Meziani, "The design and mathematical modelling of novel extensor bending pneumatic artificial muscles (EBPAMs) for soft exoskeletons," *Robotics and Autonomous Systems*, vol. 99, pp. 63-74, 2018, doi: 10.1016/j.robot.2017.10.010.

[27] R. K. Salih and W. S. Aboud, "Smart Robotic Exoskeleton: Constructing Using 3D Printer Technique for Ankle-Foot Rehabilitation," *Journal of Robotics and Control (JRC)*, vol. 4, no. 4, pp. 537-547, 2023, doi: 10.18196/jrc.v4i4.18429.

[28] H. Q. T. Ngo and M. H. Nguyen, "Enhancement of the Tracking Performance for Robot Manipulator by Using the Feed-forward Scheme and Reasonable Switching Mechanism," *Journal of Robotics and Control (JRC)*, vol. 3, no. 3, pp. 328-337, 2022, doi: 10.18196/jrc.v3i3.14585

[29] B. W. Ang and C.-H. Yeow, "Design and modeling of a high force soft actuator for assisted elbow flexion," I*EEE Robotics and Automation Letters*, vol. 5, no. 2, pp. 3731-3736, 2020, doi: 10.1109/LRA.2020.2980990

[30] J. Zhang *et al.*, "Robotic artificial muscles: Current progress and future perspectives," *IEEE transactions on robotics*, vol. 35, no. 3, pp. 761-781, 2019, doi: 10.1109/TRO.2019.2894371.

[31] K. Ashwin and A. Ghosal, "A survey on static modeling of miniaturized pneumatic artificial muscles with new model and experimental results," *Applied Mechanics Reviews*, vol. 70, no. 4, p. 040802, 2018, doi: 10.1115/1.4041660.

[32] H. A. Al-Mosawi, A. Al-Ibadi, and T. Y. Abdalla, "A Comprehensive Comparison of Different Control Strategies to Adjust the Length of the Soft Contractor Pneumatic Muscle Actuator," *Iraqi Journal for Electrical & Electronic Engineering*, vol. 18, no. 2, 2022, doi: 10.37917/ijeee.18.2.13.

[33] M. J. Bennington, T. Wang, J. Yin, S. Bergbreiter, C. Majidi, and V. A. Webster-Wood, "Design and Characterization of Viscoelastic McKibben Actuators with Tunable Force-Velocity Curves," in *2023 IEEE International Conference on Soft Robotics (RoboSoft)*, pp. 1-7, 2023, doi: 10.1109/RoboSoft55895.2023.10122014.

[34] G. Gregov, S. Pincin, A. Šoljić, and E. Kamenar, "Position Control of a Cost-Effective Bellow Pneumatic Actuator Using an LQR Approach," in *Actuators*, vol. 12, no. 2, p. 73, 2023, doi: 10.3390/act12020073.

[35] M. A. Al-Ibadi, F. K. Al-Assfor, and A. Al-Ibadi, "An Automatic Self Shape-Shifting Soft Mobile Robot (A4SMR)," *Robotics*, vol. 11, no. 6, p. 118, 2022, doi: 10.3390/robotics11060118

[36] J. Shen, T. Miyazaki, S. Ohno, M. Sogabe, and K. Kawashima, "Two Degree of Freedom Adaptive Control for Hysteresis Compensation of Pneumatic Continuum Bending Actuator," *arXiv preprint arXiv:2309.09423*, 2023, doi: 10.48550/arXiv.2309.09423.

[37] R. Kobayashi, H. Nabae, and K. Suzumori, "Large Torsion Thin Artificial Muscles Tensegrity Structure for Twist Manipulation," *IEEE Robotics and Automation Letters*, vol. 8, no. 3, pp. 1207-1214, 2023, doi: 10.1109/LRA.2023.3236889

[38] A. Aliseichik et al., "Artificial Muscles," *Journal of Computer and Systems Sciences International*, vol. 61, no. 2, pp. 270-293, 2022, doi: 10.1134/S1064230722010026.

[39] J. Mi, G. Huang, and J. Yu, "Characterization and Joint Control Study of Pneumatic Artificial Muscles," *Applied Sciences*, vol. 13, no. 2, p. 1075, 2023, doi: 10.3390/app13021075.

[40] W. Al-Mayahi and H. Al-Fahaam, "A Review of Design and Modeling of Pneumatic Artificial Muscle," *Iraqi Journal for Electrical & Electronic Engineering*, vol. 20, no. 1, pp. 122-136 2024, doi: 10.37917/ijeee.20.1.13.

[41] S. W. Khara *et al.*, "Compliant Pneumatic Muscle Structures and Systems for Extra-vehicular and Intra-vehicular Activities in Space Environment," *IET The Institution of Engineering and Technology*, 2021, doi: 10.1049/PBCE131E_ch3.

[42] H. A. Mohsen, A. Al-Ibadi, and T. Y. Abdalla, "Different Types of Control Systems for the Contraction Pneumatic Muscle Actuator," In *2022 8th International Conference on Control, Decision and Information Technologies (CoDIT)*, vol. 1, pp. 956-961, 2022, doi: 10.1109/CoDIT55151.2022.9804047.

[43] Q. Guan, J. Sun, Y. Liu, N. M. Wereley, and J. Leng, "Characterization and nonlinear models of bending extensile/contractile pneumatic artificial muscles," *Smart Materials and Structures*, vol. 30, no. 2, p. 025024, 2021, doi: 10.1088/1361-665X/abd4b0.

[44] J. S. Tate, A. D. Kelkar, and J. D. Whitcomb, "Effect of braid angle on fatigue performance of biaxial braided composites," *International journal of fatigue*, vol. 28, no. 10, pp. 1239-1247, 2006, doi: 10.1016/j.ijfatigue.2006.02.009.

[45] L. A. Al Abeach, S. Nefti-Meziani, and S. Davis, "Design of a variable stiffness soft dexterous gripper," *Soft robotics*, vol. 4, no. 3, pp. 274-284, 2017, doi: 10.1089/soro.2016.0044.

[46] L. Al Abeach, S. Nefti-Meziani, T. Theodoridis, and S. Davis, "A variable stiffness soft gripper using granular jamming and biologically inspired pneumatic muscles," *Journal of Bionic Engineering*, vol. 15, pp. 236-246, 2018, doi: 10.1007/s42235-018-0018-8.

[47] B. Kalita, A. Leonessa, and S. K. Dwivedy, "A review on the development of pneumatic artificial muscle actuators: Force model and application," in *Actuators*, vol. 11, no. 10, p. 288, 2022, doi:10.3390/act11100288 .

[48] B. Jamil, N. Oh, J.-G. Lee, H. Lee, and H. Rodrigue, "A review and comparison of linear pneumatic artificial muscles," *International Journal of Precision Engineering and Manufacturing-Green Technology*, pp. 1-13, 2023, doi: 10.1038/s41578-021-00389-7.

[49] Y. Sun, H. Feng, I. R. Manchester, R. C. H. Yeow, and P. Qi, "Static modeling of the fiber-reinforced soft pneumatic actuators including inner compression: Bending in free space, block force, and deflection upon block force," *Soft robotics*, vol. 9, no. 3, pp. 451-472, 2022, doi: 10.1089/soro.2020.0081

[50] T. Triwiyanto, W. Caesarendra, V. Abdullayev, A. A. Ahmed, and H. Herianto, "Single Lead EMG signal to Control an Upper Limb Exoskeleton Using Embedded Machine Learning on Raspberry Pi," *Journal of Robotics and Control (JRC)*, vol. 4, no. 1, pp. 35-45, 2023, doi: 10.18196/jrc.v4i1.17364

[51] N. A. Alawad, A. J. Humaidi, and A. S. Alaraji, "Observer sliding mode control design for lower exoskeleton system: Rehabilitation case," *Journal of Robotics and Control (JRC)*, vol. 3, no. 4, pp. 476-482, 2022, doi: 10.18196/jrc.v3i4.15239.

[52] Y. Zhang *et al.*, "Stiffness analysis of a pneumatic soft manipulator based on bending shape prediction," *IEEE Access*, vol. 8, pp. 82227-82241, 2020, doi: 10.1109/ACCESS.2020.2991423.

[53] L. S. Goia, A. B. Campo, and D. Colón, "Modelling, Control and Applications of Soft Pneumatic Actuators in Upper-Limb Exoskeletons: A Systematic Review," In *2022 Latin American Robotics Symposium (LARS), 2022 Brazilian Symposium on Robotics (SBR), and 2022 Workshop on Robotics in Education (WRE)*, pp. 1-6, 2022, doi: 10.1109/LARS/SBR/WRE56824.2022.9996030.

[54] O. Sokolov, A. Hošovský, and M. Trojanová, "Design, Modelling, and Control of Continuum Arms with Pneumatic Artificial Muscles: A Review," *Machines*, vol. 11, no. 10, p. 936, 2023, doi: 10.3390/machines11100936.

[55] S. Zabihollah, S. A. Moezi, and R. Sedaghati, "Design Optimization of a Miniaturized Pneumatic Artificial Muscle and Experimental Validation," in *Actuators*, vol. 12, no. 6, p. 221, 2023, doi: 10.3390/act12060221.

[56] W. Al-Mayahi and H. Al-Fahaam, "A Novel Variable Stiffness Compound Extensor-Pneumatic Artificial Muscle (CE-PAM): Design and Mathematical Model," *Journal of Robotics and Control (JRC)*, vol. 4, no. 3, pp. 342-355, 2023, doi: 10.18196/jrc.v4i3.18225.

[57] Q. Guan, J. Sun, Y. Liu, N. M. Wereley, and J. Leng, "Novel bending and helical extensile/contractile pneumatic artificial muscles inspired by elephant trunk," *Soft robotics*, vol. 7, no. 5, pp. 597-614, 2020, doi: 10.1089/soro.2019.0079

[58] T. Abrar, F. Putzu, J. Konstantinova, and K. Althoefer, "EPAM: Eversive pneumatic artificial muscle," in *2019 2nd IEEE International Conference on Soft Robotics (RoboSoft)*, pp. 19-24, 2019, doi: 10.1109/ROBOSOFT.2019.8722787.

[59] I. Zaway, R. Jallouli-Khlif, B. Maalej, and N. Derbel, "A Robust Fuzzy Fractional Order PID Design Based On Multi-Objective Optimization For Rehabilitation Device Control," *Journal of Robotics and Control (JRC)*, vol. 4, no. 3, pp. 388-402, 2023, doi: 10.1109/ROBOSOFT.2019.8722787.

[60] H. Li, J. Yao, P. Zhou, W. Zhao, Y. Xu, and Y. Zhao, "Design and modeling of a high-load soft robotic gripper inspired by biological winding," *Bioinspiration & Biomimetics*, vol. 15, no. 2, p. 026006, 2020, doi: 10.1088/1748-3190/ab6033.

[61] A. Al-Ibadi, S. Nefti-Meziani, and S. Davis, "The design, kinematics and torque analysis of the self-bending soft contraction actuator," In *Actuators*, vol. 9, no. 2, p. 33, 2020, doi: 10.3390/act9020033.

[62] A. H. Noviyanto, L. D. Septilianingtyas, and D. Rahmawati, "Design of a continuous passive motion (CPM) machine for wrist joint therapy," *Journal of Robotics and Control (JRC)*, vol. 2, no. 4, pp. 311-315, 2021, doi: 10.18196/jrc.2498.

[63] C. Suulker, S. Skach, and K. Althoefer, "Soft robotic fabric actuator with elastic bands for high force and bending performance in hand exoskeletons," *IEEE Robotics and Automation Letters*, vol. 7, no. 4, pp. 10621-10627, 2022, doi: 10.1109/LRA.2022.3194883.

[64] Y. Xu, Q. Fang, and H. Li, "Kinematic and quasi-static analysis model of a novel variable stiffness pneumatic artificial muscle," *Sensors and Actuators A: Physical*, vol. 329, p. 112815, 2021, doi: 10.1016/j.sna.2021.112815

[65] A. D. D. R. Carvalho, N. Karanth, and V. Desai, "Design and characterization of a pneumatic muscle actuator with novel end-fittings for medical assistive applications," *Sensors and Actuators A: Physical*, vol. 331, p. 112877, 2021, doi: 10.1016/j.sna.2021.112877.

[66] H. Al-Fahaam, M. Alaziz, S. Davis, and S. Nefti-Meziani, "Power Augmentation and Rehabilitation Exoskeleton Robot based on Variable Stiffness Soft Actuators," in *2020 International Conference on Electrical, Communication, and Computer Engineering (ICECCE)*, pp. 1-6, 2020, doi: 10.1109/ICECCE49384.2020.9179216.

[67] H. Al-Fahaam, S. Davis, and S. Nefti-Meziani, "Wrist rehabilitation exoskeleton robot based on pneumatic soft actuators," In *2016 International Conference for Students on Applied Engineering (ICSAE)*, pp. 491-496, 2016, doi: 10.1109/ICSAE.2016.7810241.

[68] M. Hao *et al.*, "Rehabilitation effect of intelligent rehabilitation training system on hemiplegic limb spasms after stroke," *Open Life Sciences*, vol. 18, no. 1, p. 20220724, 2023, doi: 10.1515/biol-2022-0724.

[69] H. Duan, Y. Lian, Y. Jing, J. Xing, and Z. Li, "Research progress in extracorporeal shock wave therapy for upper limb spasticity after stroke," *Frontiers in Neurology*, vol. 14, p. 1121026, 2023, doi: 10.3389/fneur.2023.1121026.

[70] M. Gandolfi, S. Mazzoleni, G. Morone, M. Iosa, F. Galletti, and N. Smania, "The role of feedback in the robotic-assisted upper limb rehabilitation in people with multiple sclerosis: A systematic review," *Expert Review of Medical Devices*, vol. 20, no. 1, pp. 35-44, 2023, doi: 10.1080/17434440.2023.2169129.

[71] C.-P. Chou and B. Hannaford, "Measurement and modeling of McKibben pneumatic artificial muscles," *IEEE Transactions on robotics and automation*, vol. 12, no. 1, pp. 90-102, 1996, doi: 10.1109/70.481753

[72] A. Al-Ibadi, S. Nefti-Meziani, and S. Davis, "Valuable experimental model of contraction pneumatic muscle actuator," in *2016 21st International Conference on Methods and Models in Automation and Robotics (MMAR)*, pp. 744-749, 2016, doi: 10.1109/MMAR.2016.7575229

[73] N. Tsagarakis and D. G. Caldwell, "Improved modelling and assessment of pneumatic muscle actuators," in *Proceedings 2000 ICRA. Millennium Conference. IEEE International Conference on Robotics and Automation. Symposia Proceedings (Cat. No. 00CH37065)*, vol. 4, pp. 3641-3646, 2000, doi: 10.1109/ROBOT.2000.845299.